Fixing the Field Joint That Failed on the Challenger

Allan J. McDonald*
Thiokol Corporation, Brigham City, Utah 84302

The Challenger accident in January 1986 led to an extensive redesign effort for the solid rocket booster. A redesign team accomplished this redesign effort and manufacture of the redesigned solid rocket motor for return to flight in 32 months. The successful flight of Discovery (STS-26R) on September 29, 1988, capped the most intense redesign and testing program conducted in solid rocket history. This paper addresses the redesign of the field joint only. Since the field joint redesign required significant time to incorporate changes to the basic steel case, NASA and the National Research Council requested that the redesign include improved safety margins in all areas of the solid rocket motor where hardware retrieved from prior flights indicated potential safety margin problems. As a result, design changes were incorporated into the solid rocket motor from stem to stern: field joint metal parts and insulation were modified; igniter chamber was modified; insulation thickness in all segments was increased; case-to-nozzle joint was redesigned; redundant and verifiable seals in the internal nozzle joints were incorporated; several ablative carbon-cloth phenolic components of the nozzle were modified; and several adhesive materials and processes used in various areas of the solid rocket motor were changed.

Background

THE original design and development of the Space Shuttle solid rocket motor (SRM) occurred during the mid-1970s. The first shuttle flight was in April 1981.[1,2] Modifications were made in that design to increase performance in the early 1980s with the design referred to as the High-Performance Motor (HPM).[3] The final configuration of the HPM first launched the shuttle in August 1983 (STS-8). A graphite epoxy filament wound case (FWC) version of the SRM[4] was also successfully developed for the Air Force Space Shuttle flights out of Vandenberg Air Force Base (VAFB), California, but this project was terminated shortly after the Challenger (STS 51-L) accident. The Space Shuttle launchsite at VAFB was "mothballed." The design discussed in this paper commenced in mid-1986, subsequent to the Challenger accident, and is referred to as the redesigned solid rocket motor (RSRM), which experienced its successful first flight on the Discovery launch on September 29, 1988. The test program for certifying the RSRM involved six times more testing and orders of magnitude more analyses than were completed in the original qualification program for the SRM prior to the maiden flight of the Space Shuttle (STS-1) in April 1981. The RSRM testing program was accomplished in less than one-half the time of the original qualification program. The RSRM was successfully static tested over the entire range of environmental temperature and flight structural loading conditions in a new large SRM test facility. The RSRM was also successfully tested with severe intentional flaws in the insulation and seal areas, demonstrating its high reliability and vastly increased margins of safety over the HPM design flown on the Challenger mission.

The SRM (Fig. 1) is the major element of the solid rocket booster (SRB), which also includes aft and forward skirts, nose cone, frustum, parachute and recovery avionics system, eight booster separation motors, a systems tunnel, external tank (ET) attach ring, and a redundant hydraulic thrust vector control (TVC) system that uses a hydrazine gas generator for actuating the movable nozzle for steering the Space Shuttle vehicle. The two SRMs provide the main thrust to lift the Space Shuttle off the launch pad to an altitude of about 155,000 ft and approximately 25 nmi. On the pad, the two SRBs support the entire weight of the Space Shuttle vehicle (approximately 4,500,000 lb) and transmit the weight load through their structure to the mobile launch platform (MLP). Each RSRM produces a maximum thrust of 3,320,000 lbf. The SRMs are ignited after the three Space Shuttle main engines (SSME) total thrust level is verified. The two RSRMs provide over 80% of the thrust at liftoff and accelerate the Space Shuttle to approximately 3000 mph before separating from the remainder of the Space Shuttle launch vehicle. Solid rocket booster apogee occurs approximately 70 s after SRB separation, at an altitude of approximately 220,000 ft and 35 nmi downrange. The three main parachutes are deployed at approximately 6300 ft. The nozzle exit cone is severed with a linear shaped charge 10 s before splashdown to reduce water impact loads. The SRBs impact the ocean 122 nmi downrange at approximately 60 mph (Fig. 2) some 7 min after launch.

The SRMs are the largest solid rocket motors ever flown, the only man-rated SRMs ever built, and the first designed for recovery and reuse. Each is 126.115 ft (1513.38 in.) long and 12.167 ft (146.00 in.) in diameter. At launch, each weighs 1,255,979 lb, of which 88% (1,107,169 lb) is propellant. The boosters are designed to be used 20 times. Each booster is attached to the ET at the SRB's aft frame by two lateral struts and a diagonal strut. The SRBs are attached to a cross beam that goes through the intertank structure to the opposite SRB; the axial thrust loads of the SRM are reacted at this location. Each booster is attached to the MLP at the aft skirt by four bolts that are severed by pyrotechnics at SRM ignition.

The propellant mixture in each motor consists of ammonium perchlorate (oxidizer, approximately 69.7% by weight), aluminum (fuel, 16%), iron oxide (a burning rate catalyst, approximately 0.3%), a polybutadiene acrylonitrile polymer (a fuel binder that holds the mixture together, 12.04%), and an epoxy curing agent (1.96%). The propellant is molded into an 11-point, star-shaped perforation in the forward portion of the forward segment that transitions into a cylindrical perforation (CP) grain in the aft portion of the forward segment. Each of the three remaining segments has aft-tapered CP grains. This configuration provides high thrust at ignition, then reduces the thrust by approximately 25% from 20 to 60 s after liftoff to prevent overstressing the vehicle during maximum dynamic pressure (max Q) and limiting flight acceleration loads to 3g.

Presented as Paper 89-2404 at the AIAA/ASME/SAE/ASEE 25th Joint Propulsion Conference, Monterey, CA, July 10-12, 1989; received Oct. 2, 1989; revision received April 20, 1990.

*Vice President, Advanced Programs and Technology, Space Operations. Associate Fellow AIAA.

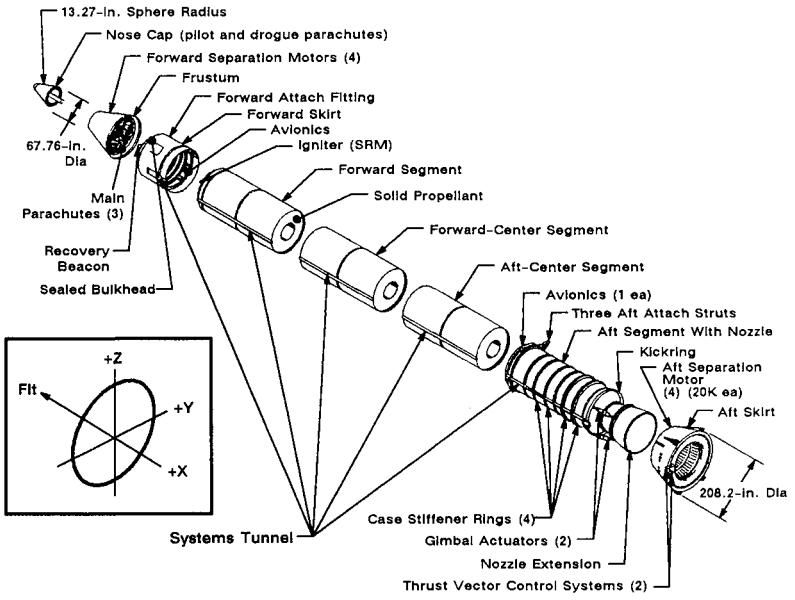

Fig. 1 Solid rocket booster (SRB).

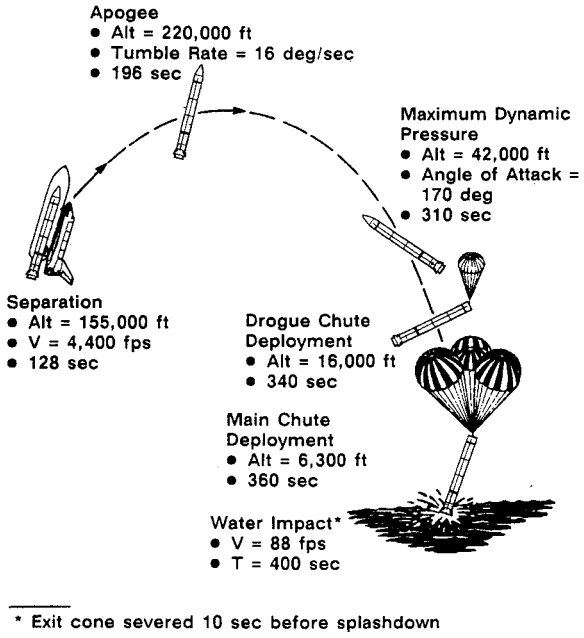

* Exit cone severed 10 sec before splashdown

Fig. 2 Typical SRB flight profile.

Table 1 RSRM performance tolerances

Parameter	Nominal	Maximum 3σ variation, % Individual motor about the nominal	Maximum 3σ variation, % Maximum difference between matched pairs
Web time, s	111.7	±5.0	2.0
Action time, s	123.4	±6.5	3.0
Web time average pressure, psia	660.8	±5.3	2.0
Maximum head end pressure, psia	918.4	±6.5	—
Maximum sea-level thrust, lbf × 106	3.06	±6.2	—
Web time average vacuum thrust, lbf × 106	2.59	±5.3	2.0
Vacuum delivered specific impulse, s	267.1	±0.7	1.0
Web time vacuum total impulse, lbf-s × 106	288.9	±1.0	1.4
Action time vacuum total impulse, lbf-s × 106	296.3	±1.0	1.4

Each RSRM is made up of four SRM casting segments. The segmented design provides maximum flexibility in RSRM fabrication, transportation, and handling. Each segment is shipped to the launchsite on a heavy duty railcar with a specially built cover. The aft exit cones are shipped on special railcars and are assembled to the primary nozzles at Kennedy Space Center (KSC). The nozzle expansion ratio of each booster is 7.72:1. Each nozzle has a carbon-cloth phenolic liner that erodes and chars during firing. The nozzle is a convergent-divergent, movable design in which an aft pivot-point flexible bearing with an 8-deg vector capability is the gimbal mechanism.

RSRM Performance

The nominal ignition interval is 231 ms from ignition command to the safety and arming (S&A) device until the chamber pressure reaches 564 psia, at which time the Space Shuttle lifts off of the MLP. The nominal propellant mean bulk temperature (PMBT) for predictions is assumed to be 60°F at ignition. The maximum rate of pressure rise is 116 psi for any 10-ms interval during the ignition transient.

Maximum allowable thrust imbalance between motors is 300,000 lbf at ignition, 85,000 lbf during motor burn, and 100,000–700,000 lbf maximum during tailoff depending upon tailoff time, with tailoff thrust imbalance impulse not to exceed 4,500,000 lbf-s. Thrust and pressure traces are shown in Figs. 3 and 4, respectively; Table 1 summarizes the RSRM nominal performance values and tolerances.

The redesign of the SRMs resulted in increasing the inert weight of each SRM by approximately 3000 lbm, with a corresponding decrease in propellant weight to improve margins of safety in nearly all areas of the motor, i.e., igniter, case insulation, field and factory joints, case-to-nozzle joint, nozzle assembly, and external insulation thermal protection systems (TPS). The overall SRM weight did not significantly change, as shown in Table 2. Reused component hardware is identified in Table 3 along with the reuse requirements.

Field Joint Design

RSRM case material is a high-strength steel alloy (D6AC) with a minimum uniaxial yield of 180,000 psi and an ultimate strength of 200,000 psi. Unlike any other rocket motor, Space

Table 2 Mass properties comparison—RSRM vs HPM

	Total RSRM, lb	Total HPM, lb
Case	98,010	97,633
Insulation	20,191	18,587
Liner	1,347	1,346
Inhibitor	1,800	1,896
Igniter inerts	485	463
Systems tunnel	533	533
Instrumentation	80	9
Joint heater cable	24	——
Nozzle-to-forward section	17,524	17,210
Propellant		
Motor	1,107,035	1,110,024
Igniter	134	137
External insulation	637	305
Items shipped separate		
Exit cone[a]	6,193	5,872
Separation system	231	260
Stiffener rings[a]	908	908
Joint heater system	348	——
Exit cone installation	22	18
S&A installation	15	15
RSRM installation	439	519
System tunnel joints	21	21
Total RSRM	1,255,979	1,255,751

[a]With external insulation installed.

Table 3 RSRM components and assemblies, minimum reusability design objectives

Component	Number of reuses
Case cylindrical segments	19
Case stiffener segments	19
Case attach segments	19
Case forward and aft closures	19
Case stiffener rings	19
Stiffener ring attach fasteners	TBD
Case clevis joint pins	19
Nozzle metal parts	19
Nozzle flex seal reinforcements	19
Shims and end mounting rings	TBD
Nozzle flex seal assembly	9
Nozzle boss attach bolts	19
S&A device	19
Igniter chamber	19
Igniter adapter	19
Chamber pressure transducers	19
Igniter port special bolts [for mounting chamber pressure monitor operational pressure transducers (OPT)]	5
Pin retainer band	TBD

Shuttle RSRM cases are designed to be recovered after use, with many of the components refurbished and reused as many as 19 times. This requires that the cases be protected against the additional loads and conditions of splashdown, recovery, and refurbishment, as well as the highly corrosive environment of the ocean. The nominal case wall or membrane thickness of the center segments is 0.479 in., as compared with the standard weight forward segment nominal case wall thickness of 0.506 in.

The RSRM case is a segmented design consisting of a hemispherical aft dome segment, two stiffener segments, an ET attach segment, six cylindrical segments, and an elliptical forward dome segment as shown in Fig. 5. Tang and clevis mechanical joints and roll-formed cylinders allow for a completely weld-free assembly. The segmented design facilitates the operations of recovery, refurbishment, propellant casting, shipping, and assembly for launch to ensure RSRM reusability for Space Shuttle missions. The case also serves as a structural element of the Space Shuttle system.

Case segment factory joints are mated before applying the insulation and liner materials. The nozzle fixed housing-to-aft dome and igniter adapter-to-forward dome joints are mated to their respective segments prior to shipment. The remaining cylindrical case joints along with the aft exit cone are mated at the launchsite as a field operation; hence, these are called field joints (Fig. 6).

Metal Parts

Case casting segments are joined by the RSRM capture feature tang- and clevis-type field joints. These three joints, located between the four casting segments, are assembled for flight at the launchsite. The RSRM and HPM field joint configurations are compared in Fig. 7. New features incorporated into the design include a capture feature with a third O-ring, modified O-ring grooves, a 45-deg positioned leak test port, and a vent port at the 135-deg position with custom shims and a volume filler. Leak check and vent ports are perpendicular to the case walls, with reduced (0.625-in. diameter) through-hole dimensions. The vent port provides for the release of air that would otherwise be trapped between the capture feature and primary O-rings during assembly, and also provides for the leak checking of those O-rings and the positioning of the primary O-ring.

An interference fit exists between the capture feature and the clevis inner leg. This interference fit minimizes the gap opening between the joint sealing surfaces and also provides a tremendous heat sink with minimal flow area if gases were to ever reach this area. Considering worst-on-worst conditions, the interference fit controls inter-O-ring gap opening to approximately 0.009 in. maximum as compared to 0.051 in. for the HPM.

The RSRM load-bearing pin design includes a hole through the pin to assist in assembly. The pin has been lengthened from 1.43 to 1.65 in., and the dovetail on the inner end of the new pin has been lengthened. The remaining dovetail is outboard of the outer clevis leg outside diameter (o.d.) in an area outside of the high-stress area. The pins are made from

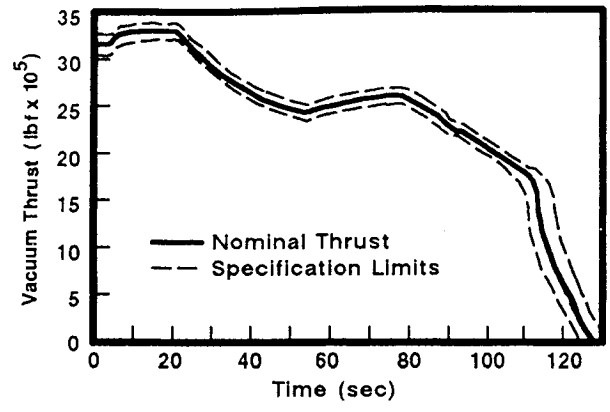

Fig. 3 Nominal RSRM thrust vs time curve.

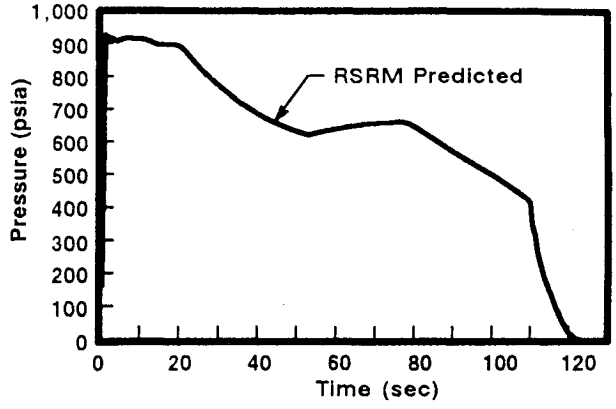

Fig. 4 RSRM pressure vs time.

nonferrous MP35N nickel alloy, having an ultimate tensile strength of 260,000–305,000 psi. Custom shims are inserted around each pin in each joint to fill the gap between the o.d. of the tang and the i.d. of the outer clevis leg. After joint mating, the gaps are measured at each pin location. The specific shim thickness is selected to conform to the average of the measured gaps. The shims slip around each pin in the gap. Their purpose is to ensure a uniform gap around the motor case circumference for the O-ring seals. The material used for the shims is Inconel 718 that is heat treated to ensure a minimum strength of 180,000 psi. After a joint is mated and the 177 pins and shims are installed to complete the structural integrity of the joint, a retainer band is installed over the pins. This band is fabricated from Inconel 718 and is designed to a breaking load of 9650 lb. The Inconel material is solution heat-treated to a maximum ultimate tensile strength of 180,000 psi. The band is fabricated in three equal length sections. The sections are joined at the trunnion by bolts. The hat shape of the retaining band is designed to rest on the top of the pins, providing a positive pin restraint and preventing the band from longitudinal movement.

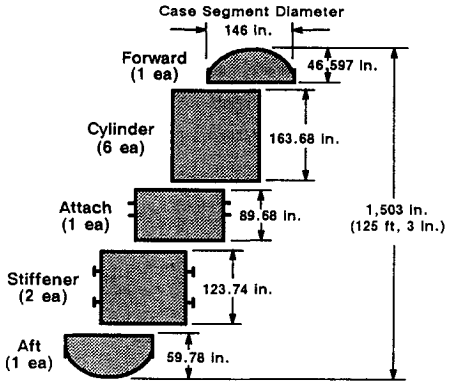

Fig. 5 RSRM case segments.

All of the clevis joints of the RSRM have been modified to provide interchangeability and assembly with the new capture feature tang hardware. The inner clevis leg surface has been machined to provide a seal surface for the capture feature O-ring. The transition over the slope at the end of the inner clevis leg has been smoothed. The slope has been changed from an angle of 17 deg, 30 min, to 18 deg, 30 min. The inner clevis leg end has been thinned by 0.010–0.015 in. to assist segment mating, to provide for a new vent port plug for capture feature/primary O-ring leak checking, and to ensure primary O-ring seating. The width of the O-ring grooves has been increased from 0.305–0.310 in. to 0.355–0.360 in. The nominal slope of the O-ring groove has been changed from 5 to 12 deg. The O-rings have also been changed from seals with a nominal diameter of 0.280 in. to seals having a nominal diameter of 0.290 in. A chamfer on the outer clevis leg has also been machined into the RSRM design.

Insulation

The case field joint insulation design is an unvented J-joint configuration (see Fig. 7). The J-joint insulation configuration is vulcanized as an integral part of the insulation system. The leg of the tang insulation is fabricated in a deflected position. The deflected leg was designed to ensure that during assembly (under worst thermal conditions, propellant slump, manufac-

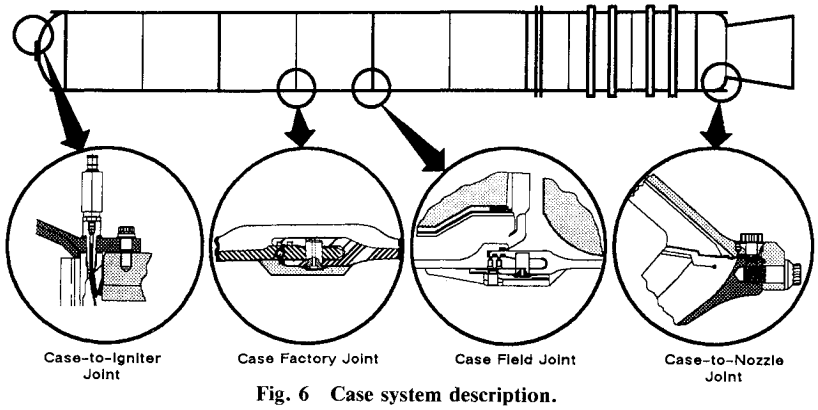

Fig. 6 Case system description.

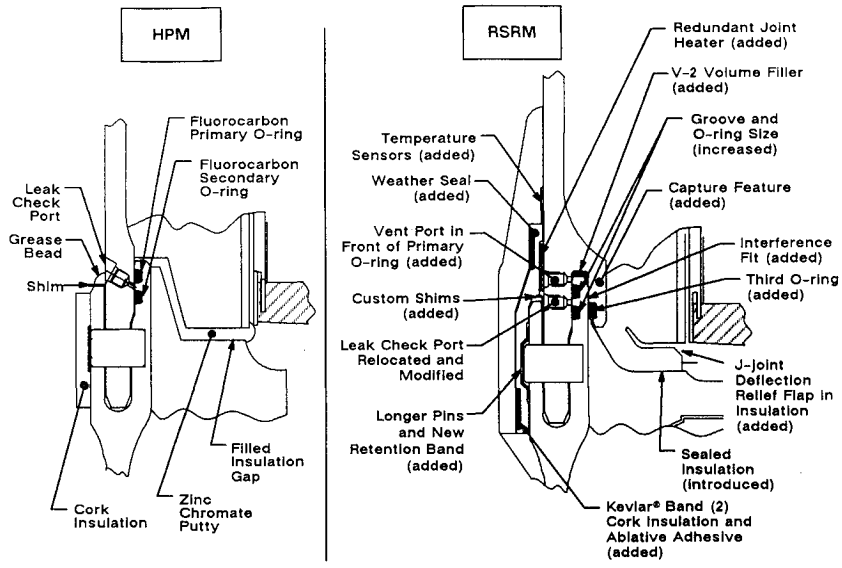

Fig. 7 Field joint comparison.

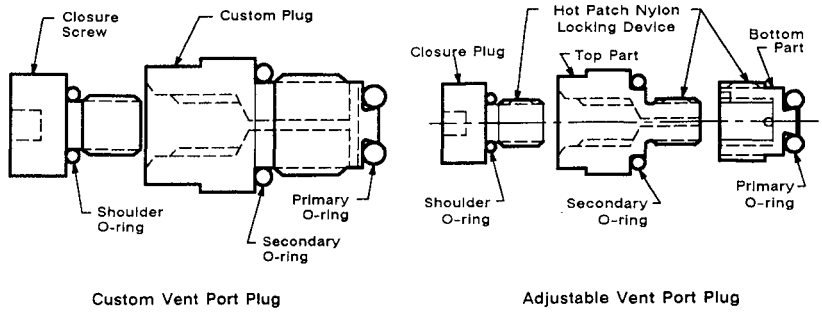

Fig. 8 Vent port plugs.

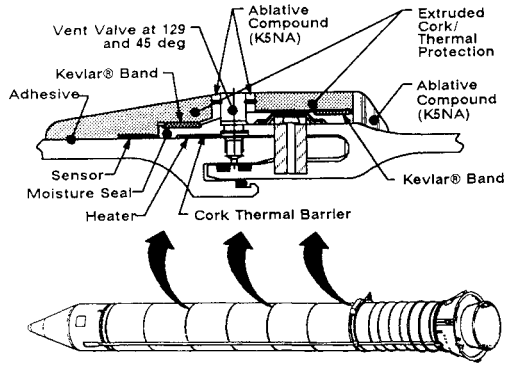

Fig. 9 Field joint protection system.

turing tolerances, and joint tolerances) compressive contact between the tang and clevis insulation mating surfaces would be provided and maintained. At motor ignition, the gap of the J-joint is pressurized, forcing the deflected leg against the bond to the clevis insulation, thus increasing joint compressive contact and reducing the amount of free volume downstream in the J-joint. The J-joint also provides a stress relief mechanism enabling the joint insulation to accommodate joint movement and thermal cycling of the propellant grain. The field joint insulation configuration incorporates the use of a thin pressure-sensitive adhesive bondline. The unvented J-joint configuration was designed to prevent hot chamber gases from reaching and damaging the O-ring seals, to provide an insulation joint bond, and to meet insulation performance safety-factor requirements of 2.0 minimum, based on material decomposition depth.

Seal Design

The field joint has been significantly modified in the RSRM design as was shown in Fig. 7. In the capture feature of the joint, a third barrier O-ring has been added. This O-ring always responds in an opposite manner to the two O-rings in the inner clevis leg, providing true seal redundancy. The capture feature O-ring along with the J-joint insulation tend to close tighter during pressurization of the motor. In the capture feature, immediately forward of the barrier O-ring, a metal-to-metal interference fit has been built into the design. In the upper end of the inner clevis leg, a fluorocarbon V_2 volume filler in eight sections of 54.3 in. each is positioned in the capture feature tang with 2.5-in. gaps between each section. The gaps permit venting during assembly and the leak checking of the primary O-ring-to-capture feature cavity.

The leak check port for the primary/secondary O-ring cavity has been moved from the 0-deg position to the 45-deg position and repositioned directly in the joint. Pressure into this cavity properly positions the secondary O-ring in its groove. A new vent port has been located at the 135-deg position on the case wall to pressure test the primary/capture feature cavity and, in so doing, properly positions the primary O-ring.

The HPM field joint was pressurized to 200 psia between the primary and secondary O-ring; pressure was then reduced to 50 psia for leak checking that consisted of 1-psia drop in 10 min. The RSRM field joint seal leak testing provides for an initial test in the cavity between the primary and secondary O-rings, using a maximum expected operating pressure (MEOP) of 1000 ±10 psi. The pressure decay is monitored and the leak rate compared to allowable. At the same time, pressure rise is monitored between the primary seal and the capture feature O-ring. Then the cavity between the primary and secondary seal is tested at low pressure (30 ±3 psi). Again, the leak rate is calculated from pressure decay data and compared with the allowable rate. When the primary to secondary leak test has been completed, the primary to capture feature O-ring cavity is leak tested at 100 ±5 psi. Simultaneously, the primary to secondary cavity is monitored for pressure rise. Finally, the primary to capture feature cavity is tested at low pressure, 30 ±3 psi, while the primary to secondary cavity is monitored. This leak check process will detect contamination in the O-ring seal area at low pressures and also prevent grease from masking O-ring flaws at high pressures.

A number of requirements exist for all seal testing. Proper positioning of the O-ring seals in the grooves is a requirement. To protect metal sealing surfaces from the possibility of rust or corrosion, all of them are coated with HD-2 corrosion preventive grease. The HD-2 grease is carefully controlled so as not to affect leak checking of the seals. To preclude the introduction of gaseous contamination into the joint areas (humidity, etc.), gaseous inert nitrogen is employed in all leak testing applications. All leak test equipment is certified as to accuracy before being used to test the joints. All threads on leak test plugs have nylon locking mechanisms.

Fluorocarbon V1115 was the material selected after extensive testing of O-ring materials. This material is an improved version (by omission of a filler material, extensive production controls, and material property requirements) from the Viton 747, fluorocarbon O-rings used in the HPM design. The material is compatible with the HD-2 grease, does not absorb significant quantities of nitrogen gas, has acceptable resilience, functions well in high-temperature environments, has good surface hardness for assembly requirements, has consistent and acceptable material properties, and has good spliceability. Other candidate materials did not possess all of these properties. Reduced joint rotation, along with temperature control of the joint, makes the fluorocarbon O-ring material the most reliable O-ring material.

Port Plugs

Vent plugs have been added to the field joints between the primary and capture feature O-rings. They serve the purpose of venting air from the joint during assembly, providing for leak checking, and for proper positioning of the primary O-rings. Since this port is a potential primary leak path, vent port plugs are required to be sealed with a redundant and verifiable plug (Fig. 8).

The adjustable vent port plugs were used in most applications after the second flight because they provide for independent seating of the seals and can accommodate variations in port depths. Both the custom and adjustable plugs have closure plugs and three O-ring seals. The primary O-ring is used

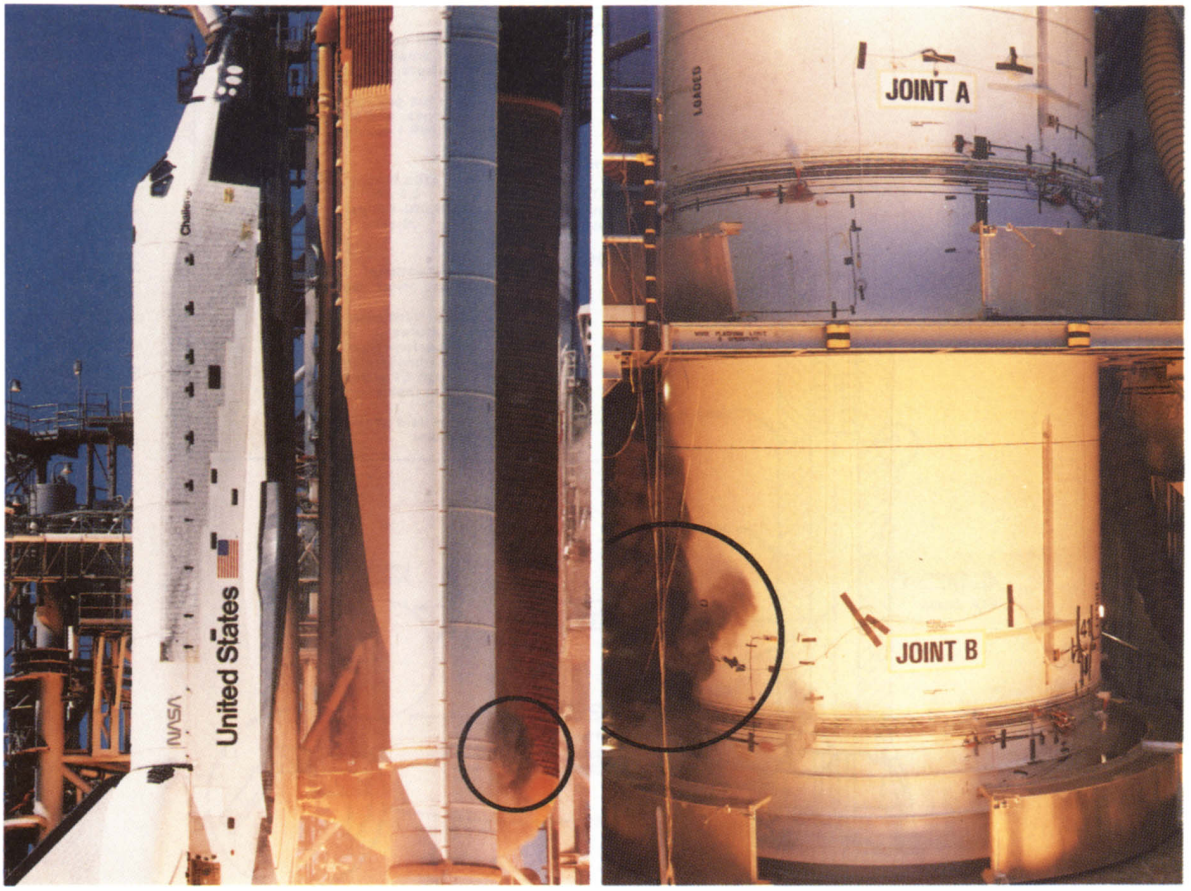

Fig. 10 Duplication of Challenger joint failure.

as a packing seal. There are two shoulder-type secondary seals. The custom plug is fitted to each port to allow adequate compression on the primary O-ring and complete seating of one secondary O-ring when fully installed. Both plugs are closed out after leak checking with the closure plug which is not verified. Both types of plugs provide for nylon locking devices.

Leak check port plugs are used to close all leak check ports. All of them use shoulder-type seals in a port hole configuration. The seals are not required to be redundant since the primary O-ring of the joints act as the primary seal with the leak check port shoulder seals acting as the redundant seal. A Nylok locking mechanism is incorporated in all plug designs. Two different size plugs are used: 0.2500-28 UNJF and 0.4375-20 UNF.

Joint Protection System

The Joint Protection System (JPS) was designed to provide a method of keeping the field joint O-rings at their optimum sealing temperature. The system provides a weather seal during Space Shuttle ground operations and acts as a moisture seal during recovery operations. The JPS must also provide thermal protection for the segment assembly pin retainer band.

Because of the criticality of field joint performance and the conditions of field assembly of the joint, the field joint JPS in Fig. 9 has five major components:

1) A joint heater and thermal barrier to maintain the O-ring temperature to at least 75°F minimum.

2) A temperature-sensing system for monitoring the temperatures of the joint surface.

3) An ethylene-propylene-diene monomer (EPDM) moisture seal and Kevlar retainer band to compress the heater against the case wall, provide heater insulation and protection, and to provide a positive seal of the joint against water intrusion.

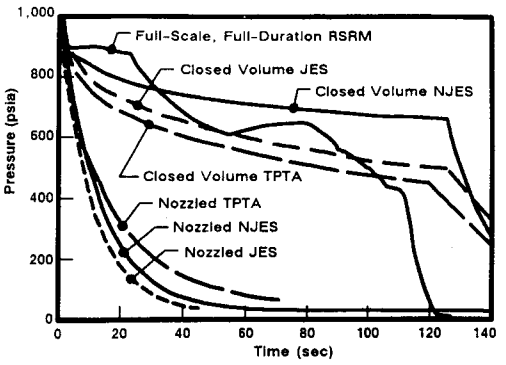

Fig. 11 Pressure/time traces for short-burn tests.

4) A vent valve to release entrapped air as the vehicle passes out of Earth's atmosphere, while precluding entry of air or sea water upon re-entry and splashdown.

5) Cork thermal protection that encompasses all of the joint components.

The heater is designed to maintain the temperature of the O-rings at 75°F minimum while the RSRM is on the launch pad prior to launch. The heater is assembled to the case wall immediately adjacent to the outer clevis leg, over the tang, with pressure-sensitive adhesive to hold it in position for assembly. It has a cutout over the 135-deg leak check port. The one-piece heater assembly contains a primary and redundant heater. The two-piece sensor assembly contains four separate sensors. The heater operates on 208 Vac facility power and produces 3500 W. The heater shielding is grounded to the motor case with ground straps.

Since the joint heater is not required after liftoff, the heater and sensor cables feature breakaway connectors at the aft skirt umbilical. Power for the heaters comes from the ground sup-

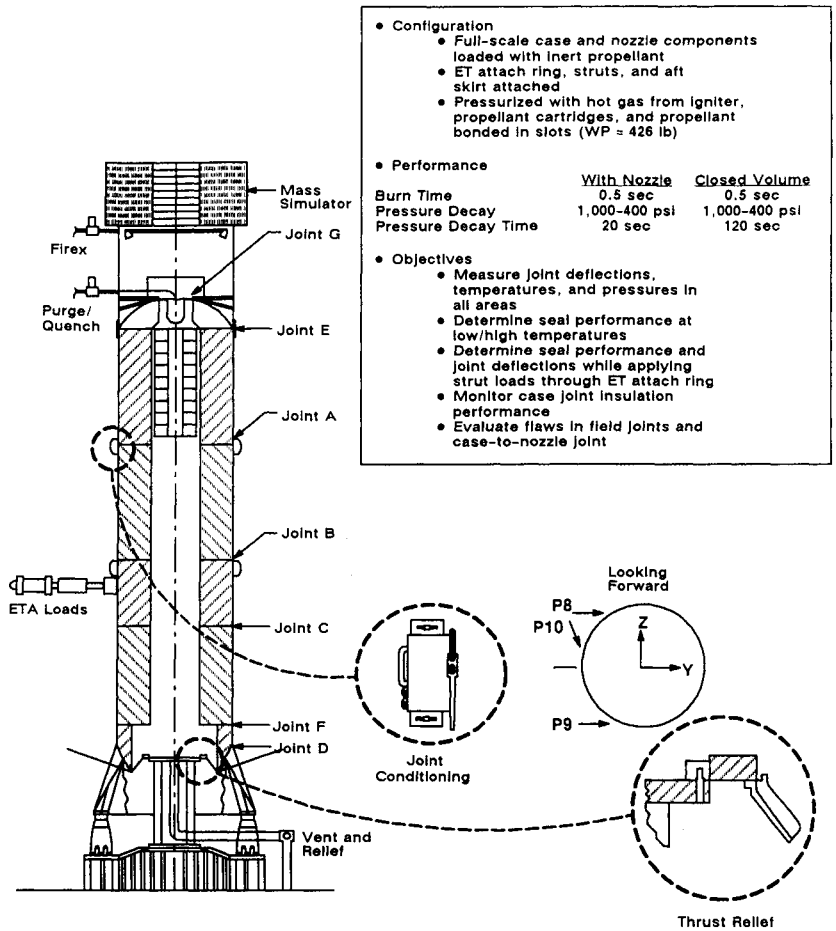

Fig. 12 TPTA configuration.

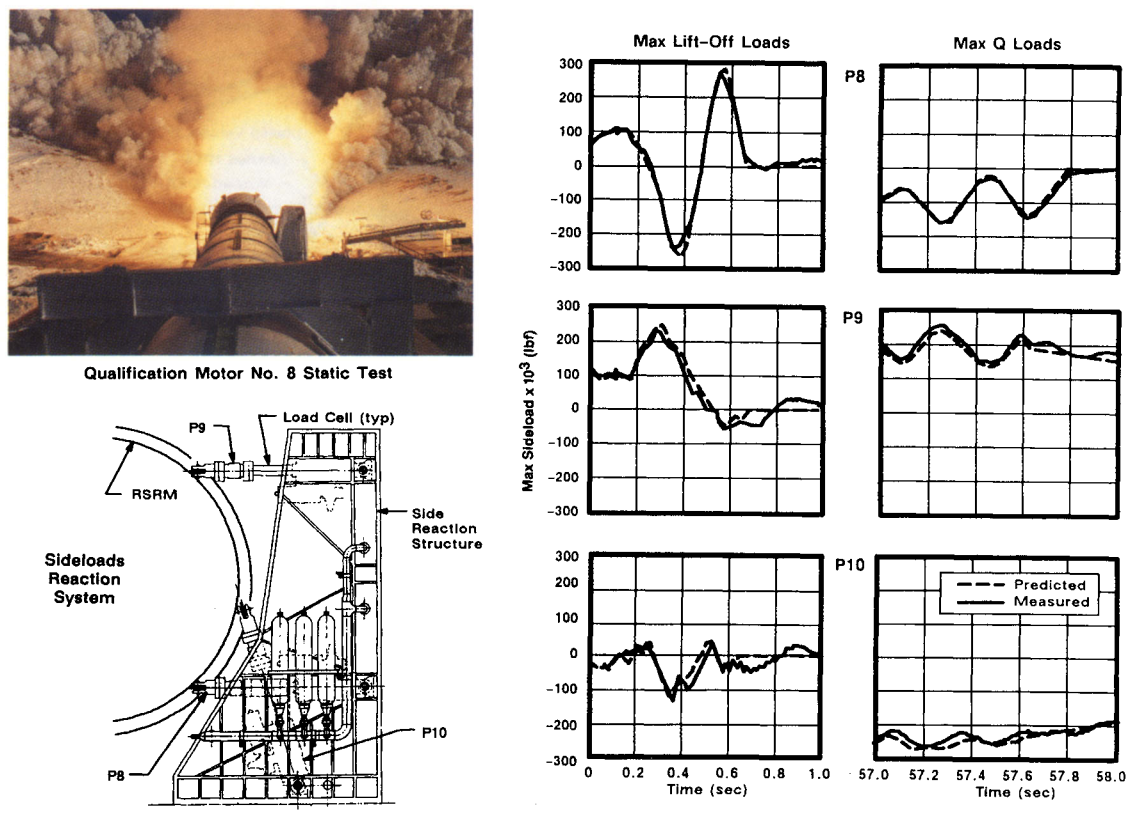

Fig. 13 Qualification motor no. 8 cold static test (PMBT = 39°F) with sideloads applied.

port equipment through the liftoff umbilical to cables mounted into the aft skirt to the aft plug plate.

Design Verification

The RSRM was fully certified by a comprehensive test program. This test program incorporated many new and innovative test articles for verification of the new joint designs. Highly instrumented joint environment simulators were developed for providing a better understanding of joint behavior under various thermal and structural loading conditions. The primary workhorse for this testing was the joint environment simulator (JES), which was first used in duplicating the aft field joint failure experienced by the Challenger (Fig. 10) when subjected to unusually cold prelaunch temperatures (20 ± 5°F). The joint simulators used full-scale hardware with sufficient live propellant and either a small nozzle or closed volume to simulate the ignition transient of a full-duration motor (Fig. 11). A nozzle joint environment simulator (NJES) was also developed for verifying the new case-to-nozzle joint design.

A more sophisticated version of the JES was tested at NASA's Marshall Space Flight Center (MSFC). This test motor, designated a transient pressure test article (TPTA), featured an aft stiffener segment on the ET attach section, with three hydraulic struts attached to the ET attach ring to input dynamic strut loads during ignition and time of max Q. The TPTA also featured the redesigned case-to-nozzle joint as part of the test assembly, an aft skirt, and a mass simulator on top weighing over a million pounds to represent the weight of the entire shuttle system supported by the SRBs on the MLP at time of launch (Fig. 12).

The test program included 18 full-scale, short-burn tests of the various joint simulators; 76 hot-fire tests of subscale motors; 14 assembly tests, including a long-term (one year) J-joint stacking test; 4 structural hydrotests, including a burst test of the redesigned case-to-nozzle joint; a structural test ar-

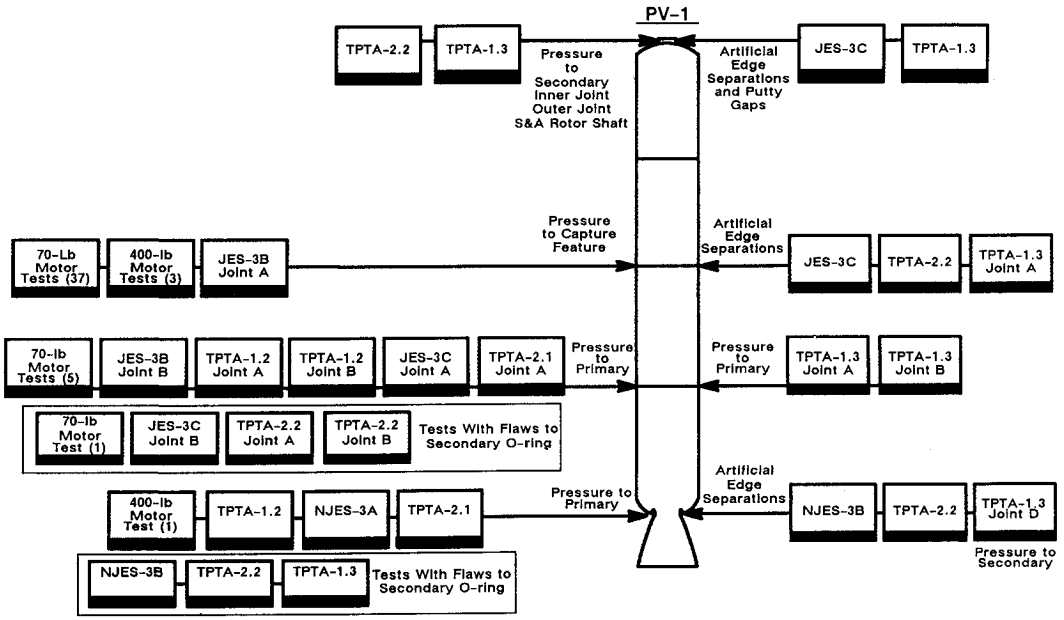

Fig. 14 Flaw test summary.

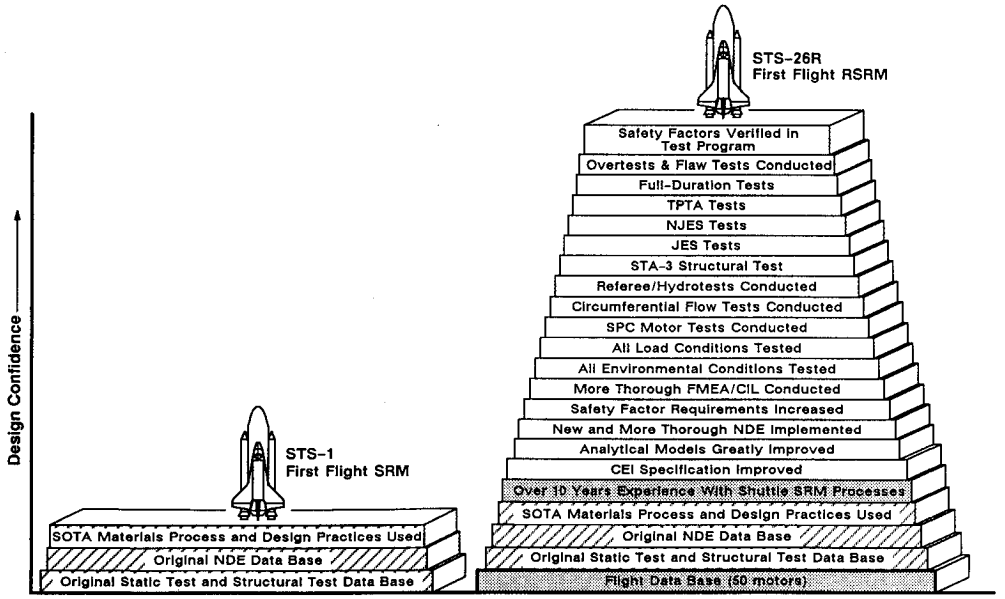

Fig. 15 Test program confidence for first flight of RSRM (STS-26R).

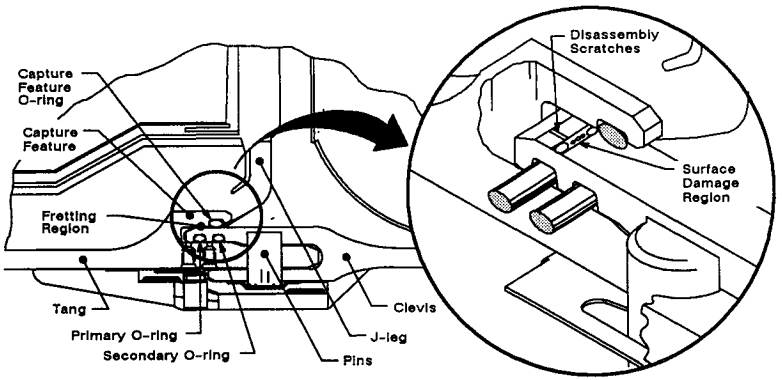

Fig. 16 RSRM case field joint fretting.

ticle subjected to prelaunch, pressure, and flight ultimate loads; 2 modal survey tests; and 6 full-duration RSRM static tests, including two tests at the required temperature extremes (40-90°F PMBT) with design liftoff and max Q flight loads applied through the struts on the ET attach ring (Fig. 13). Actual PMBTs achieved in these two tests were 39 and 92°F; external skin temperatures were as low as 29°F in the cold motor test and 119°F in the hot motor test.

The test program also included flaw testing the insulation and seals in the joint areas to demonstrate the significant increase in joint safety margins. Flaw testing was conducted on numerous joint environment simulators and subscale motors prior to introducing severe flaws in a full-duration RSRM certification test motor—production verification motor no. 1 (PV-1)—prior to first flight (Fig. 14). Flaws were created by intentionally cutting holes through the J-joint insulation in two field joints in order to allow hot gas to reach the capture feature O-ring and also by cutting away most of the capture feature O-ring in one of the joints to allow hot gas to reach the primary O-ring. Similar flaws were created in the case-to-nozzle joint to allow hot gas to reach the wiper O-ring and beyond to the primary O-ring. The primary case insulation was intentionally separated from the case at the edge of the insulation in these areas of hot-gas penetration as well. Although this test was intended to demonstrate fail-safe operation, the PV-1 motor performed within specifications even with these severe flaws. The flaw testing program was unprecedented in the solid rocket industry. These highly instrumented motors provided over 11,000 channels of engineering data. The design confidence for the first flight of the RSRM (STS-26R) in September of 1988 as compared to the design confidence of the first flight of the Space Shuttle in April of 1981 is illustrated in Fig. 15.

Conclusions

Results from the extensive ground test program and microscopic examination of returned flight hardware from the first nine launches of the Space Shuttle have confirmed the vastly improved margins of safety of the RSRM.

The first three flights of the Space Shuttle wih the RSRM (STS-26R, -27R, and -29R) included development flight instrumentation (DFI). The instrumentation data along with the engineering evaluation of the disassembled hardware from static and flight tests have confirmed the design improvements in the RSRM. The only anomaly noted to date has been the presence of numerous small fretting corrosion pits (0.001–0.013 in. deep) on several of the tang and clevis legs of the field joints in the area of interference (Fig. 16). This anomaly did not manifest itself in the static test program and is, therefore, currently being investigated. It is not known whether fretting is occurring as a result of rollout to the pad, ascent-pressurized flight, unpressurized re-entry, or splashdown and towback. The fretting corrosion pits are in a low stress area and do not represent a flight-safety concern, but they could possibly impact hardware reuse assignments in the future.

References

[1]Thirkill, J. D., "Solid Rocket Motor for the Space Shuttle Booster," AIAA/SAE 11th Propulsion Conference, Sept. 29–Oct. 1, 1975, Anaheim, CA.

[2]Dorsey, E. G., Jr., "The Space Shuttle Solid Rocket Motor," 33rd Congress of the International Astronautical Federation, Sept. 27–Oct. 20, 1982, Paris, France.

[3]Bailey, L. G., Nichols, G. E., and Saderholm, C. A., "Space Shuttle Rocket Motor Performance Improvement," 1983 JANNAF Propulsion Meeting, Feb. 1983, Monterey, CA.

[4]McDonald, A. J., "Design Evolution of the Space Shuttle Solid Rocket Motors," AIAA Paper 85-1265, July 1985.